arXiv:cond-mat/0502617v1 [cond-mat.soft] 25 Feb 2005

Structural Order in Glassy Water

Nicolas Giovambattista[1], Pablo G. Debenedetti[1],

Francesco Sciortino[2], and H. Eugene Stanley[3]

[1] *Department of Chemical Engineering,*

Princeton University, Princeton, NJ 08544-5263 USA

[2] *Dipartimento di Fisica and INFM Udr and SOFT: Complex Dynamics in Structured Systems*

Universita' di Roma "La Sapienza" – Piazzale Aldo Moro 2, I-00185, Roma, Italy

[3] *Center for Polymer Studies and Department of Physics*

Boston University, Boston, MA 02215 USA

(22 February 2005)

Abstract

We investigate structural order in glassy water by performing classical molecular dynamics simulations using the extended simple point charge (SPC/E) model of water. We perform isochoric cooling simulations across the glass transition temperature at different cooling rates and densities. We quantify structural order by orientational and translational order metrics. Upon cooling the liquid into the glassy state, both the orientational order parameter Q and translational order parameter τ increase. At $T = 0$ K, the glasses fall on a line in the Q-τ plane or *order map*. The position of this line depends only on density and coincides with the location in the order map of the inherent structures (IS) sampled upon cooling. We evaluate the energy of the IS, $e_{IS}(T)$, and find that both order parameters for the IS are proportional to e_{IS}. We also study the structural order during the transformation of low-density amorphous ice (LDA) to high-density amorphous ice (HDA) upon isothermal compression and are able to identify distinct regions in the

order map corresponding to these glasses. Comparison of the order parameters for LDA and HDA with those obtained upon isochoric cooling indicates major structural differences between glasses obtained by cooling and glasses obtained by compression. These structural differences are only weakly reflected in the pair correlation function. We also characterize the evolution of structural order upon isobaric annealing, leading at high pressure to very-high density amorphous ice (VHDA).

I. INTRODUCTION

Crystalline solids are characterized by a periodic structure and, therefore, by the presence of long range-oder. A well-defined theoretical and experimental framework is available for characterizing the structure of crystals [1]. On the other hand, numerous materials found in nature and widely utilized in technology exist in an amorphous state (e.g., glasses and liquids) [2]. Characterizing the structure of amorphous materials is a challenging task because such systems organize over short distances and show no long-range order. Moreover, the local structure in such materials is not unique and it can change throughout the sample. Therefore, new tools are required to characterize the structure of amorphous materials. One promising approach is to develop order metrics (order parameters) that quantify certain statistical properties of the structure [3]. Recent work in this direction has been performed on the hard-sphere [4,5] and Lennard-Jones (LJ) [6] particle systems. Structural order was characterized with two metrics: a translational order parameter τ quantifying the tendency of particle pairs to adopt preferential separations, and a bond-orientational order parameter Q quantifying correlations between the bond angles defined by a given particle and its nearest neighbors. The novelty of this approach resides not in the order metrics themselves, which have been used before (e.g., [7]), but in the idea of an *order map*, in which different states are mapped onto a plane whose axes represent the order metrics [4,5]. The order map for the Lennard-Jones and hard-sphere systems consists of a line, indicating that the two

order metrics are not independent [5,6].

Extension of these ideas to liquid water has proven to be most useful. In Ref. [8], the structural order of cold liquid water was investigated and found to be closely related to the well-known dynamic [9–11] and thermodynamic [12] anomalies of this substance. It was found that there exists a region in the phase diagram bounded by loci of maximum orientational order and minimum translational order within which the dynamic and thermodynamic anomalies occur. Water's order map was found to be more complex than for simpler, spherically-symmetric systems. State points define a *two-dimensional region* in the order map, implying that orientational and translational order are in general independent. Remarkably, however, it is found that the region where water exhibits dynamic or thermodynamic anomalies defines a *line* in the order map, which implies that when water behaves anomalously, its translational and orientational order metrics are no longer independent, but are instead strictly correlated. This property was then used to quantify threshold values of the order metrics needed in order for various anomalies to occur [8]. Similar (though not identical) behavior was found to occur in another tetrahedral liquid, silica [13].

Notable among water's peculiarities is the fact that it exhibits polyamorphism [14–16], i.e., the presence of more than one glassy form. Uniaxial compression of ice-I_h [17] or ice-I_c [18,19] at $T = 77$ K to pressures $P \gtrsim 1$ GPa produces a disordered high-density material named high-density amorphous ice (HDA). If HDA is recovered at $T = 77$ K and $P = 1$ bar and then heated isobarically, it transforms irreversibly at $T \approx 125$ K to a disordered low-density material named low-density amorphous ice (LDA) [17,20]. Moreover, LDA transforms to HDA when compressed at $T = 77$ K to $P = 0.6$ GPa [20,21]. The LDA-HDA transformation is reversible above $T \approx 130$ K [22]. Furthermore, because it is very sharp and shows hysteresis, it has been suggested that the LDA-HDA transformation is a first-order transition [22–24]. The LDA-HDA transition plays a central role in one of the thermodynamically-consistent scenarios that have been proposed to explain the experimentally observed properties of supercooled water [16].

There are several other routes to producing amorphous ice [14–16] in addition to those

mentioned above. Because glasses are non-equilibrium materials, their properties are history-dependent, and the specific procedure followed in the glass preparation may lead to different amorphous forms. It is not clear whether all the different amorphous ices can be classified into two *families* [25–27], one corresponding to LDA and the other to HDA. One complication standing in the way of such a satisfyingly simple view is the experimental observation that HDA, when annealed or heated at high pressure becomes appreciably denser. The resulting glass is called very-high density amorphous ice (VHDA) or relaxed HDA (RHDA) [28]. Whether VHDA/RHDA is simply yet another form of glassy water or whether, as suggested by simulations [29,30], it is the more stable form to which HDA relaxes irreversibly is a question currently under investigation.

It should be evident from the preceding discussion that a precise characterization of structural order in water glasses is of considerably interest. The purpose of the present work is to provide such a characterization. In particular, (i) we use the order metric approach introduced in [8] for equilibrium liquid water to quantify structural changes that occur when liquid water is cooled isochorically to the glassy state; (ii) we quantify the changes in structural order that accompany the LDA→HDA transformation; (iii) we investigate structural evolution during the annealing/isobaric heating of the amorphous ices obtained upon compression of LDA; and (iv) we compare the location in the order map of the various glasses obtained in (i), (ii) and (iii). By doing this, we are able to characterize *quantitatively* structural differences between samples of amorphous ice obtained by different procedures. In recent related work, Guillot and Guissani [31] performed computer simulations of glassy water obtained along different paths. They used the radial distribution function and structure factor to study the structure of the different glasses. In this work, we instead use the order map approach. As we show below, this approach allows a precise and sensitive characterization of structure.

This work is organized as follows. In the next Section, we present the simulations details. In Section III, we study the local structure when the liquid is cooled isochorically across the glass transition at different cooling rates and for different densities. We study both

the structure in the instantaneous configurations and in the corresponding potential energy minima attained by steepest descent mapping (inherent structures, IS). In Section IV, we study the evolution of structural order during the LDA→HDA transformation, and upon annealing (i.e., isobaric heating) different glasses obtained during the compression procedure. The comparison of the local structure of the glasses obtained with the different procedures mentioned above is discussed in Section V. We present the conclusions in Section VI.

II. SIMULATIONS

We perform classic molecular dynamics (MD) simulations of a ($N = 216$)-molecule system using the extended simple point charge (SPC/E) model of water [32]. This model has been extensively used to study the thermodynamics [10,33] and dynamics [34,35] of liquid water and is consistent with experimental facts (e.g., at low temperatures it exhibits density anomalies [36] and a diffusivity that increases upon compression [10]). The SPC/E model has also been used to study glassy water, and is able to produce glassy states corresponding to LDA, HDA and VHDA [30,37].

To cool the liquid to the glass state, we perform constant volume simulations at $\rho =$ 0.9, 1.0, 1.1, 1.2, 1.3 and 1.4 g/cm^3. At each density we average the results over 16 independent simulations (with the exception of $\rho = 1.00$ g/cm^3 where we use 32 independent simulations). We use periodic boundary conditions and the reaction field method (with a cutoff of 0.79 nm) to treat the long range forces. Upon cooling at each density, we change the T by rescaling the velocities of the molecules using the Berendsen thermostat [38]. At every time step $\delta t = 1$ fs, we decrease the thermostat temperature by $\delta T = q_c \delta t$, where $q_c < 0$ is the cooling rate. Cooling simulations starting from an equilibrium liquid at $T = 300$ K down to $T = 0$ K are performed with cooling rates $q_c = -30, \ -10^2, \ -10^3, \ -10^4$ and -10^5 K/ns. Similar values for q_c have been used in previous simulations at $\rho = 1.00$ g/cm^3 to study the effect of cooling and heating rates on the glass transition temperature $T_g = T_g(P)$ [39,40]. The glass obtained with a cooling rate $q_c = -30$ K/ns behaves, upon heating at $q_h =$

+30 K/ns, as an experimentally slow-cooled glass, and shows no signs of hyperquenching effects [40]. On the other hand, the smallest cooling/heating rates accessible nowadays in computer simulations are $|q| \approx 10$ K/ns [31].

To study the evolution of structural order during the LDA→HDA transformation, we perform compression simulations at $T = 77$ and 170 K and average results over 16 independent trajectories at each temperature. We perform MD simulations at constant ρ for intervals of 1 ps and at the end of each interval we increase ρ by $\delta\rho = 5 \times 10^{-5}$ g/cm^3. These ρ changes are performed by rescaling isotropically the coordinates of the molecular center of mass. Therefore, our compression rate is $\delta\rho/\delta t = 5 \times 10^{-5}$ g/cm^3/ps. This value was already used to study the potential energy landscape region sampled during the LDA-HDA transformation [37]. We also perform 16 independent compression simulations at $T = 0$ K; at each simulation step we change ρ by $\delta\rho = 5 \times 10^{-5}$ g/cm^3 and then minimize the energy. At each step, ρ is modified by rescaling isotropically the center of mass of each molecule.

We stress that our results are relative to the cooling/compression rates studied here. However, the cooling/compression rates we use are such that the compression run ($0.9 \leq \rho \leq 1.4$ g/cm^3) and the slowest cooling run ($300 \geq T \geq 0$ K) both take 10 ns, i.e. both numerical 'experiments' are based on the same time scale (as is expected to be the case in an experiment).

The annealing procedure of the glasses obtained upon compression consists of isobaric MD simulations where the temperature is increased from $T = 77$ K (i.e., the compression temperature used in the LDA→HDA transformation) up to $T = 170$ K. We use the Berendsen thermostat [38] to fix the T, and at every time step $\delta t = 1$ fs, we increase the thermostat temperature by $\delta T = q_h \delta t$, where $q_h = +30$ K/ns is the heating rate. A coupling to an external bath at a given P (analogous to the Berendsen thermostat) is used to keep the pressure constant [38]. We perform annealing runs at $P = -0.55, \ -0.17, \ 0.01, \ 0.41, \ 0.68, \ 0.84, \ 1.10, \ 1.38$ and 1.90 GPa and average results over 16 trajectories.

We also investigate structural order in mechanically stable configurations sampled during

isochoric cooling. These configurations are local potential energy minima called inherent structures (IS). To obtain the IS we perform energy minimizations by using the conjugate gradient algorithm. We consider the minimization complete when the change in energy between two successive minimizations is $\leq 10^{-15}$ kJ/mol.

We compute for the glasses the same translational and orientational order parameters τ and Q introduced in [8] to study structural order in liquid water. The translational order parameter τ is given by

$$\tau \equiv \frac{1}{\xi_c} \int_0^{\xi_c} |g_{OO}(\xi) - 1| d\xi \tag{1}$$

where $\xi \equiv r\rho_n^{1/3}$ is the distance between the oxygen atoms of pairs of molecules, r, divided by the mean nearest-neighbor separation at the number density $\rho_n \equiv N/V$; $g_{OO}(r)$ is the oxygen-oxygen radial distribution function (RDF) and $\xi_c \equiv 2.843$ is a cut-off distance. In an ideal gas, the RDF is equal to 1 and $\tau = 0$. In a crystal, there is long-range order and $g_{OO}(r) \neq 1$ over long distances, and τ is large.

The orientational order parameter Q is given by

$$Q \equiv 1 - \frac{3}{8} \sum_{j=1}^{3} \sum_{k=j+1}^{4} \left(\cos\psi_{jk} + \frac{1}{3} \right)^2 \tag{2}$$

where ψ_{jk} is the angle formed by the lines joining the oxygen atom of a given molecule and those of nearest neighbors j and k (≤ 4). For the purpose of this calculation, we limit our attention to the four oxygen atoms that are closest to a given oxygen atom. This definition is a slightly modified version of the metric introduced in Ref. [41]. Equation (2) implies that $-3 \leq Q \leq 1$. In an ideal gas, $< Q >= 0$ (where $< ... >$ denotes an ensemble average) [8]. In a perfect tetrahedral network $\cos(\psi_{jk}) = -1/3$, and $Q = 1$. Thus, Q measures the degree of tetrahedrality in the distribution of the four nearest oxygen atoms around a central oxygen atom.

III. STRUCTURAL ORDER UPON ISOCHORIC COOLING

A. Instantaneous Configurations

Figure 1(a) shows the evolution of the order parameters Q and τ during cooling of an initially equilibrated liquid at constant density $\rho = 1.00$ g/cm^3 from $T = 300$ K down to $T = 0$ K. We show the results for different cooling rates q_c and include the line obtained in [8] separating the accessible and the inaccessible regions for *equilibrium liquids*. No equilibrium liquid states of the SPC/E model exist in the range 220 K$\leq T \leq$ 400 K and 0.85 g/cm$^3\leq$ $\rho \leq 1.3$ g/cm^3 with order parameter combinations (Q, τ) to the right of this limiting line.

The starting location of the system in the ordering map is indicated by the square symbol 'A' and is in agreement with the values reported in [8] for a liquid at $T = 300$ K and $\rho = 1.0$ g/cm^3. Upon cooling at the slower rate $q_c = -30$ K/ns, the system moves in the order map along the line delimiting the accessible region for the liquid state and finally, at approximately $T = 240$ K, the system departs from this line and moves into the accessible region. The boundary between the accessible and inaccessible regions is the locus of state points where structural, dynamic, and thermodynamic anomalies occur [8]. Equilibrium liquid states that display structural, dynamic, or thermodynamic anomalies (decrease of both τ and Q upon isothermal compression; increase in diffusivity upon isothermal compression; decrease in density upon isobaric cooling, respectively) are therefore characterized by only one order parameter (*line* in the Q-τ plane). In contrast, liquid states that do not exhibit anomalies are characterized by two order parameters (accessible *area* in the Q-τ plane) [8]. Therefore, at $\rho = 1.0$ g/cm^3 and 300 K $\geq T \geq$ 240 K, the equilibrium liquid experiences a cascade of anomalies (first structural, then dynamic, finally thermodynamic) upon cooling [8]. For $T <$ 240 K, the quenched liquid falls out of equilibrium and in so doing moves into the accessible region of the order map. We use the term equilibrium to denote states where the structural relaxation time is short compared to the simulated time at the given T and ρ. Equilibrium states for the liquid at $\rho = 1.0$ g/cm^3 and 220 K$\leq T \leq$ 300 K lie on the

limiting line separating the accessible and inaccessible regions [8].

In order to understand the trajectory followed by the quenched system at $\rho = 1.00$ g/cm^3 in the order map we note that the liquid is able to reach equilibrium during cooling down to $T \approx 240$ K. The structural relaxation time at $T > 240$ K is $t_r < 30$ ps [10] while during the cooling process, the typical time scale for the system to relax before T changes by 1 K is $dt = 1$ K$/|q_c| \approx 33$ ps $\approx t_r$. For $T < 240$ K, therefore, the system is not able to reach equilibrium upon cooling (i.e., $dt < t_r$) and it attains, for a given Q, larger values of τ than those possessed by the liquid in equilibrium at the given T and ρ. Equivalently, the quenched system attains smaller values of Q, for a given τ, than those of the equilibrium liquid at the given T and ρ.

It is interesting to study the behavior of the thermodynamic properties when the system falls out of equilibrium upon cooling. Figure 1(b) shows the behavior of pressure P as a function of T upon cooling at $q_c = -30$ K/ns and $q_c = -10^4$ K/ns. As a guide to the eye, we also include data from equilibrium simulations taken from Ref. [33]. Upon cooling at $q_c = -30$ K/ns the pressure clearly follows the equilibrium $P(T)$ trend, showing a minimum at $T \approx 250$ K. A minimum in $P(T)$ at constant density corresponds to a maximum in $\rho(T)$ at constant density (see e.g. [10]). Therefore, upon cooling at $q_c = -30$ K/ns, the liquid is able to experience a density anomaly $[(\partial P/\partial T)_\rho < 0]$ in the approximate range 250 K$\geq T \geq$ 190 K, whereas for the equilibrium liquid, density anomalies occur for all $T \leq 250$ K. When the liquid is cooled faster, at $q_c = -10^4$ K/ns, the pressure deviates from the equilibrium $P(T)$ curve at a comparatively higher T. No signature of a density anomaly is observed when cooling at this high rate. This suggests that configurations responsible for producing density anomalies possess comparatively larger equilibration times. This observation warrants a systematic investigation. We note that pressure fluctuations make it difficult to estimate the T at which the instantaneous P deviated from the equilibrium $P(T)$ curve.

The phenomenology discussed above when relating the behavior of the order parameters upon cooling at $q_c = -30$ K/ns is common to all the cooling rates studied [see Fig. 1(a)]. However, we observe that the larger $|q_c|$, the higher the T at which the system falls out of

equilibrium (i.e., the earlier the system deviates from the line delimiting the inaccessible region). Furthermore, the larger is $|q_c|$, the closer are the final values of Q and τ to those of the starting liquid (square symbol 'A' in the figure), meaning that the structure of the glass is more similar to that of the starting liquid. Equivalently, the smaller is $|q_c|$, the more structured is the final glass, i.e., the larger the final values of Q and τ.

The long-dashed line in Fig. 1(a) is the locus of Q-τ values for $\rho = 1.0$ g/cm^3 glasses obtained at $T = 0$ K with the five q_c studied. Interestingly, such isochorically-quenched glasses define a line in the order map. We note that these results are similar to simulations performed using a Lenard-Jones potential [43]. In fact, Fig. 7 in that work shows that upon isochorically cooling a liquid with different cooling rates, the orientational and translational parameters increase monotonically with decreasing cooling rate, and the glasses obtained at the lowest T fall on a straight line with positive slope in the order map, just as we find for SPC/E water.

The features observed at $\rho = 1.00$ g/cm^3 are also found at all the other densities studied, i.e., $\rho = 0.9,\ 1.1,\ 1.2,\ 1.3$, and 1.4 g/cm^3. The results for $\rho = 1.3$ g/cm^3 are shown in Fig. 1(c). In agreement with [8], comparison between Figs. 1(a) and (c) indicates that the location in the order map of the starting liquid at $T = 300$ K (square symbol) depends on the density. Furthermore, at the high density $\rho = 1.3$ g/cm^3 the equilibrium liquid does not exhibit structural, dynamic, or thermodynamic anomalies. Accordingly, the quench trajectories in the order map do not attain the line separating the accessible and inaccessible regions. We note that at all the densities and cooling rates studied, the glasses always remain out of the inaccessible region obtained previously for the equilibrium liquids [8]. In this respect, the inaccessible region in the order map seems to be the result of topological constrains inherent in the molecular interactions and does not depend on whether the system is in the liquid or glassy state.

The radial distribution function is one of the standard tools used in experiments, theory, and simulations to characterize the structure of condensed matter. We show in Fig. 2 the oxygen-oxygen radial distribution function $g_{OO}(r)$ for the glasses obtained at $T = 0$ K upon

cooling at $\rho = 1.00$ g/cm^3 with the same five cooling rates shown in Fig. 1(a). These glasses are located in the order map along the long-dashed line. While differences in the structures of the glasses are suggested by both Fig. 1(a) and Fig. 2, the differences observed in $g_{OO}(r)$ are quite subtle and could be difficult to distinguish from typical experimental error bars. It therefore appears that the location of the system in the (Q, τ) *order map* is a sensitive indicator of glass structure. Same conclusion holds when comparing $g_{OO}(r)$ for the glasses obtained upon compression of LDA at $T = 0$ K (where no annealing is possible) and the isochorically fast-quenched glasses at the same T. For example, inset of Fig. 2 compares the $g_{OO}(r)$ for the glass obtained upon isothermal compression at $T = 0$ K to $\rho = 1.0$ g/cm^3 and for the isochorically quenched glass at $q_c = -10^5$ K/ns at the same density and temperature. The glasses obtained by isothermal compression and those prepared by other routes will be discussed and compared in detail in the rest of the paper. The point here, though, is to emphasize that the differences in $g_{OO}(r)$ shown in the inset of Fig. 2 are quite subtle, whereas the two glasses have very different order metrics: $Q = 0.83$, $\tau = 0.57$ for $T = 0$ K-compression of LDA; $Q = 75$, $\tau = 50$ for the isochorically-quenched glasses at $q_c = -10^5$ K/ns.

B. Inherent Structures

We now investigate the location in the order map of the IS sampled by the system upon cooling from $T = 300$ K down to $T = 0$ K. We denote the tetrahedral and translational order parameter of the IS by Q_{IS} and τ_{IS}, respectively.

Figure 3(a) shows the evolution of Q and τ upon cooling the liquid at $\rho = 1.00$ g/cm^3 at $q_c = -30$ K/ns [taken from Fig. 1(a)]. For each configuration obtained from the MD simulations, we find the corresponding IS and then calculate the order parameters Q_{IS} and τ_{IS}. The evolution of Q_{IS} and τ_{IS} upon cooling at $q_c = -30$ K/ns are also indicated in Fig. 3(a). Interestingly, we find that the Q_{IS} and τ_{IS} values fall on the same line that characterizes the glasses obtained upon cooling isochorically to $T = 0$ K at different q_c

[long-dashed line in Fig. 1(a); included also in Fig. 3(a)]. In fact, we find that for all the IS obtained at $\rho = 1.00$ g/cm^3 from systems quenched at *any* quenching rate q_c, the parameters Q_{IS} and τ_{IS} fall on the same line that characterizes the isochorically-quenched glasses at $T \approx 0$ K [see Fig. 3(b)]. We also note that the values of the order parameters are larger in the IS than in the liquid (i.e., the IS are more structured than the liquid configurations).

In Fig. 3(c) we show that the behavior found at $\rho = 1.00$ g/cm^3 occurs at all densities studied. For each density, there is a line in the order map that characterizes the location of the IS sampled upon cooling, which coincides with the location of the glasses at $T = 0$ K. The location of each of these lines depends non-monotonically on ρ. At low ρ, the IS-line is located at high Q and τ. As density increases, this line moves toward lower values of Q and τ, and finally, at high ρ, it shifts to lower values of Q but larger values of τ. The range of order parameters sampled by the IS shrinks appreciably upon compression within the range of q_c values studied.

From Ref. [8], it is found that equilibrium liquid states of a given density fall on a single curve in the (Q, τ) plane. Therefore, it is interesting to investigate how this equilibrium liquid line compares to the corresponding IS line at the same density. This is done in Fig. 3(d) where we show the location in the order map of the equilibrium liquid at different ρ (from Ref. [8]) and the lines shown in Fig. 1(c) for the corresponding ρ. Clearly, for a given ρ the equilibrium liquid line differs from the corresponding IS line.

The finding that the Q_{IS}-τ_{IS} values fall on a density-dependent line in the order map has the following implications: (i) Q_{IS} and τ_{IS} are not independent for a fixed density, i.e., one cannot change the average orientational order in the IS without changing the translational order; (ii) the function $\tau_{IS}(Q_{IS})$ is independent of the cooling rate, i.e., on the glass history; and (iii) the function $\tau_{IS}(Q_{IS})$ is independent of whether the IS corresponds to a system in equilibrium or out of equilibrium. Conclusions (ii) and (iii) are unusual since expressions relating properties of the IS sampled by the system in equilibrium do not necessarily apply to IS sampled by the system out of equilibrium. For example, the dependence of basin curvature on IS depth has been found to be different in IS sampled by equilibrium liquids

than in IS obtained from fast-quenched or fast-compressed glasses [40,44], and to depend on the cooling/compression rates.

In the potential energy landscape (PEL) approach, any property of an equilibrium system [45] or of a system not too far from equilibrium [40,44,46] is known once the energy (e_{IS}), local curvature ($\mathcal{S}_{IS}$), and pressure of the IS (P_{IS}) are determined [45]. We investigate the connection between these properties and the structural order parameters τ_{IS}-Q_{IS}. To do this, Fig. 4(a) shows $1-Q_{IS}$ as a function of T at $\rho = 1.00$ g/cm^3 for all q_c (similar results are obtained for τ_{IS}). This figure is reminiscent of the behavior of e_{IS} observed in simulations of a Lenard-Jonnes system [47] and in water [40] upon cooling an equilibrium liquid, and suggests that $1 - Q_{IS} \approx e_{IS}$ (similarly, we find that $1 - \tau_{IS} \approx e_{IS}$) meaning that both Q_{IS} and τ_{IS} are a measure of the basin depth e_{IS} in the PEL. This is confirmed by Fig. 4(b) where we show $1 - Q_{IS}$ as a function of e_{IS}.

IV. STRUCTURAL ORDER OF LOW-DENSITY, HIGH-DENSITY AND ANNEALED AMORPHOUS ICE

A. Low-density and High-density Amorphous Ice

Next, we study the structural order parameters in glassy water. Specifically, we focus on the values of Q and τ corresponding to the glasses obtained during the LDA→HDA transformation. We *quantify* the tetrahedrality and translational order of both groups of glasses and identify regions in the order map corresponding to LDA and HDA. So far, such a characterization has been missing.

Figure 5(a) shows the ρ-dependence of pressure P during the LDA→HDA transformation at the compression temperatures of $T = 0,\ 77$, and 170 K, which lie below the glass transition locus $T_g(P)$ for this system, as determined by the behavior of $C_P(T)$ upon heating (not shown). In experiments, LDA is obtained by isobaric heating of HDA at $P = 1$ atm. In computer simulations LDA has been obtained by isochoric cooling of a low-density liquid [42,48].

Following [42,48], we obtain the starting LDA by *isochoric* fast-cooling of an equilibrium liquid at $T = 220$ K. The procedure followed to obtain LDA should not alter qualitatively our results (see Appendix). In Fig. 5(a), LDA corresponds to the linear behavior of $P(\rho)$ at low-ρ. The transformation of LDA to HDA starts at the end of this linear regime and is indicated on the left side of the figure. It is not so clear when the transformation to HDA is complete, in particular because there are aging/annealing effects [26]. For simplicity, in the following analysis we assume that HDA corresponds to the glasses obtained by compression whose density exceeds $\rho_0 \equiv 1.3$ g/cm^3. The location of these glasses in the $P - \rho$ plane is indicated in Fig. 5(a).

Figure 5(b) shows the evolution in the order map of the glasses obtained during the LDA$\rightarrow$HDA transformation. The isotherms in Fig. 5(b) correspond to those shown in Fig. 5(a). The symbols in each case denote the densities 0.9, 1.0, 1.1, 1.2, 1.3, and 1.4 g/cm^3. At the three temperatures studied, the orientational order decreases monotonically upon compression, i.e., the glasses become less tetrahedral. However, the translational order parameter behaves non-monotonically, exhibiting a minimum in the range from 1.25 to 1.3 g/cm^3. An increase in translational order upon compression is the expected behavior for a condensed-phase system [4–6]. In liquid water, this behavior occurs only at high densities [8]. It can be seen from Fig. 5(b) that the same is true in glassy water.

It is interesting that LDA and HDA are in well-defined and non-overlapping regions of the order map. The difference in tetrahedrality is especially notable, with LDA-like glasses having Q values ≥ 0.8 and HDA-like glasses having Q values approximately < 0.7. We also note that the compressed glasses remain in the accessible region of the order map.

B. Annealed Amorphous Ice

Recently, it has been found that upon annealing or heating isobarically samples of HDA at high-P, the glass becomes denser [49]; the resulting glass is called very-high-density glass (VHDA) or relaxed HDA (RHDA) [26,29,30]. VHDA/RHDA can also be obtained in

computer simulations using the SPC/E [30] and the TIP4P models [29]. In fact, it has been found [26] that annealing effects are present upon heating not only HDA, but also LDA and intermediate glasses in the LDA→HDA transformation. Figure 6(a) shows $P(\rho)$ during compression of LDA at $T = 77$ K and $T = 170$ K. We also indicate the effect of isobarically heating nine different glasses from $T = 77$ K up to $T = 170$ K [26] at pressures ranging from $P = -0.55$ up to 1.9 GPa (in the case of $P = -0.55$, the maximum T reached is $T = 160$ K). Upon heating, the density of the compressed glasses shifts from the ($T = 77$ K)-isotherm (open circles) to the full diamonds located near the ($T = 170$ K)-isotherm.

The changes in structural order that occur during annealing/isobaric heating of the nine glasses indicated in Fig. 6(a) are shown in Fig. 6(b). The effect of annealing LDA is mainly to reduce the translational order while only slightly reducing the orientational order. This is clear from the isobaric heating of LDA, at $P = -0.55$, -0.17, and 0.01 GPa [trajectories starting from the first three circles (high-Q) of the 77 K-isotherm in Fig. 6(b)]. However, as P is increased approaching the LDA→HDA transformation region, the tetrahedral order becomes more sensitive to annealing. This is clear from the heating at $P = 0.41$ GPa, which corresponds to a glass located at the end of the LDA region in Fig. 6(a) [trajectory starting from the fourth circle in Fig. 6(b)]. Although the order parameters indicate a considerable change in structure, in the case of the isobaric heating at $P = 0.01$ GPa, the density of the glass barely changes.

In contrast to the behavior observed upon isobaric heating of LDA, annealing HDA mainly reduces the orientational order, while small changes in τ are found to occur. This is clear from the isobaric heatings at $P = 1.38$ and 1.9 GPa. [trajectories starting from the last two circles (low-Q) of the 77 K-isotherm in Fig. 6(b)]. We note that in the case of the isobaric heating at $P = 1.9$ GPa, there is actually an increment in translational order, the opposite effect to that observed upon heating LDA. In the case of isobaric heating at intermediate pressures (approximately 0.41 GPa $< P <$ 1.38 GPa), both the translational and orientational order parameters decrease appreciably.

We stress that upon annealing HDA ($P = 1.38$ and 1.9 GPa), i.e. during the

HDA→VHDA transformation, the location of the glass in the order map shifts to a low-Q subregion already included in the HDA domain. Similarly, annealing LDA ($P = -0.55, \ -0.17$, and 0.01 GPa) shifts the location of the glass in the order map to a low-τ subregion already included in the LDA domain. This does not apply to glasses of intermediate densities (0.98 g/cm^3 $< \rho <$ 1.25 g/cm^3, approximately) which cannot be characterized as LDA or HDA before annealing. These systems start from, and evolve toward, an intermediate-Q region in the order map ($\approx 0.7 \leq Q < 0.8$).

A salient feature of Fig. 6(a) and 6(b) is the similarity, both in density and in structural order, between isobarically annealed glasses at $T = 170$ K and isothermally ($T = 170$ K) compressed glasses at the same density.

V. COMPARISON OF STRUCTURAL ORDER IN ISOTHERMALLY COMPRESSED, ISOBARICALLY ANNEALED, AND ISOCHORICALLY COOLED GLASSES

A. Isochorically Cooled Glasses and the Low-density and High-density Amorphous Ices

We first compare structural order in LDA and HDA with that in isochorically-quenched glasses (Section III) at the same density. To avoid aging effects, we compare the glasses obtained upon compression of LDA at $T = 0$ K to the isochorically-cooled glasses obtained also at $T = 0$ K. The location of these isochorically-quenched glasses in the $P - \rho$ plane is indicated by open symbols in Fig. 7(a). Full symbols denote the glasses from the LDA→HDA isothermal compression at $T = 0$ K. Clearly, glasses obtained upon compression have very different pressures than isochorically-cooled glasses of the same density over the range of compression and cooling rates explored here. In fact, we find that the glasses obtained by compression of LDA (at the present compression rate) at a given ρ are less stable than those obtained by slow cooling at the same density. In other words, e_{IS} for the compressed glasses

is higher than for the isochorically cooled glasses at $q_c = -30$ K/ns.

These glasses are also different structurally. In Fig. 7(b) we compare the evolution of the isothermal LDA→HDA compression at $T = 0$ K in the (Q, τ) plane with the corresponding location of isochorically quenched glasses. The LDA→HDA compression is represented by the irregular curve. For the isochorically-quenched glasses we show the (Q, τ) coordinates of the slowest- and fastest-cooled glasses ($q_c = -30$ K/ns, high-Q end; $q_c = -10^5$ K/ns, low-Q end, respectively), joined by a straight line, along which lie the glasses cooled at intermediate rates [see, e.g., Fig. 1(a)]. The symbols denote different densities, as indicated in the figure.

Among the low-ρ isochorically-cooled glasses ($\rho = 0.9$ and $\rho = 1.0$ g/cm^3), only those cooled at the slowest rates ($q_c = -30$ and $q_c = -10^2$ K/ns) fall inside the LDA region. For $|q_c| > 10^2$ K/ns we find that the structure corresponds to glasses lying between LDA and HDA in the (Q, τ) plane. As previously shown [40], glasses obtained at rates $|q_c| > 10^2$ K/ns are highly metastable and as soon as they are heated, they relax toward those glasses obtained by slower cooling rates.

At high densities, $\rho > 1.2$ g/cm^3, isochorically-quenched glasses do not fall into the HDA region in the order map, as one would expect based on their density. Even the slow-cooled glasses are located in the region between that of LDA and HDA. This again highlights the fact that the glasses obtained by compression in the LDA→HDA transformation are structurally quite distinct from those obtained by isochoric cooling (at least with the cooling and compression rates accessible with the present computer times).

In fact, we have found (results are not shown here) that e_{IS}, $\mathcal{S}_{IS}$, and P_{IS} of the glasses obtained upon isochoric cooling at a given density and those obtained upon compression of LDA at the same density can be very different and are very sensitive to the cooling rate. A similar situation seems to happen when comparing glasses obtained upon isobaric cooling with those from the LDA→HDA transformation. For example, VHDA/RHDA can be obtained upon isobaric cooling only upon fast-cooling while HDA is not accessible upon isobaric cooling of the liquid [30].

B. Isochorically Cooled Glasses and the Annealed Amorphous Ices

Figure 8(a) shows the location in the P-ρ plane of the annealed/isobarically heated glasses indicated in Fig. 6(a) (diamond symbols) and of the glasses cooled isochorically down to $T = 170$ K at different cooling rates (open symbols). Comparison of Fig. 7(a) and 8(a) shows that at this relatively high temperature, equation-of-state differences between glasses formed by different routes, though still evident, are much less pronounced.

The location in the order map of the glasses indicated in Fig. 8(a) is shown in Fig. 8(b). For comparison, we also include the location of the glasses obtained by isothermal compression at $T = 170$ K (long-dashed line). The annealed glasses are structurally very similar to those obtained upon isothermal compression, i.e., these glasses fall on the $T = 170$ K-compression curve in Fig. 8(b).

We also show in the same figure the "isotherms" connecting glasses formed by isochoric cooling at the same rate. Symbols identify the quench rate, and along each "isotherm" the density increases monotonically from 0.9 g/cm^3 (high-Q end) to 1.4 g/cm^3 (low-Q end) in 0.1 g/cm^3 increments. Note that neighboring points along an "isotherm" are not connected by a continuity of states, but were instead attained by isochoric quenches at different densities. In all these cases, Q decreases monotonically upon compression, while τ decreases initially up to $\rho \approx 1.0$ g/cm^3 and increases thereafter. With exception of the isotherms corresponding to the fastest cooling rates ($q_c = -10^4, \ -10^5$ K/ns), the low-density portions ($\rho \leq 1.25$ g/cm^3) of all the curves collapse onto a common isotherm. We thus find that glasses with 0.9 g/cm$^3 \leq \rho \leq 1.3$ g/cm^3, when sufficiently hot, share with the cold equilibrium liquid the remarkable feature [8] of having only one independent order parameter, it being impossible to change one (e.g., Q) without changing the other.

We note, finally, that at high enough densities, appreciable structural differences between glasses formed by different routes are evident even when their thermal properties are very similar. For example, all the isochorically cooled glasses at $\rho = 1.3$ g/cm^3 are at almost the same P [see Fig. 8(a)]. However, Fig. 8(b) shows that these glasses have very different order

parameters (next-to-last open symbols on each isotherm, on the low-Q end).

VI. CONCLUSIONS

In this work we have used order metrics Q and τ and the order map concept [4–6,8], to quantitatively characterize structural order in glassy states of the SPC/E model of water. Our main findings are recapitulated below.

At a given density, glasses formed by isochoric cooling down to $T = 0$ K define a line in the order map. This line shifts non-monotonically across the order map upon changing the density, and corresponds also to the location in the (Q, τ) plane of the IS sampled by the system both *in and out of equilibrium*. The finding that the order parameters of the IS fall (for a given density) on a line in the order map implies that Q and τ are not independent. In fact, we find that both Q and τ are linear functions of the depth of the IS, i.e. e_{IS}.

We have also investigated in detail the structural order of the glasses formed upon isothermal compression across the LDA→HDA transformation. At the three temperatures studied (0, 77 and 170 K), the orientational order decreases monotonically upon compression. However, the translational order decreases until $\rho \approx 1.3$ g/cm^3 (approximately, the HDA formation density); further compression increases the translational order. We were able to identify two non-overlaping and well-defined regions: a high-Q and high-τ region corresponding to LDA, and a low-Q and low- or intermediate-τ region, corresponding to HDA.

Annealing (i.e., isobaric heating) of compressed glasses is important experimentally: it has been found that it can change dramatically their properties [25,49,50]. Accordingly, we also have studied the evolution of structural order in isobarically-annealed glasses over a wide range of P. We find that annealing LDA not only decreases the density but also causes a significant decrease in translational order, while the orientational order barely changes. Annealing HDA (this corresponds to the HDA→VHDA/RHDA transformation [29,30,49]), reduces the orientational order appreciably, and causes a slight increase in translational order. While structural changes upon annealing are significant, they do not cause LDA or

HDA to move outside of their respective regions in the order map (defined *before* annealing).

We compared the structure of glasses formed by different routes in order to test whether we can relate the LDA/HDA glasses with those obtained by isochoric cooling at the same density (at least, with the present cooling/compression rates available in computer simulations). The structure of the glasses formed by different routes can be compared by traditional methods, e.g., the oxygen-oxygen radial distribution function $g_{OO}(r)$, or, alternatively, by the order map characterization utilized here. When comparing the structure of isochorically cooled, and compressed glasses at same T and ρ, we find that the location in the order map is very sensitive to structural changes. Among isobarically-cooled glasses at $T = 0$ K and $\rho = 0.9$ or 1.0 g/cm^3, only those cooled at the slowest rates ($q_c = -30$ and -10^2 K/ns) fall into the LDA region in the order map. In the case of the isochorically-cooled glasses at $T = 0$ K and $\rho = 1.3$ or 1.4 g/cm^3, they fall outside of the HDA region in the order map. Therefore, isochorically-cooled glasses in the appropriate density range cannot always be classified as LDA or HDA.

In contrast to the pronounced path-dependence of the structure of 'cold' glasses, we find much weaker history dependence in the properties of glasses formed after isobaric annealing at $T = 170$ K, when compared with those attained by isochoric cooling glasses down to the same T. Both the annealed and slow-cooled glasses are structurally very similar, and they are located in the order map on the same isotherm as compressed glasses at $T = 170$ K. We also find that glasses formed by isochoric cooling to $T = 170$ K collapse onto a common 'master' isotherm in the order map regardless of their density as long as $|q_c| < 10^4$ K/ns.

As a final observation, we note that all the glasses obtained in this work, under any condition and procedure fall in the accessible region of the order map, as found in [8] for liquid water. This suggests that the inaccessible region (at least for systems lacking long-range order) is a consequence of constrains inherent to the molecular interactions and is not dependent on whether the system is a liquid or a glass.

In this work we have applied the order map methodology to the investigation of structural order in water glasses. We find that location in the order map is a sensitive descriptor of

structure. We further find that at low enough temperature, glasses obtained by isochoric cooling are very different from those formed by isothermal compression, even when compared at the same density and temperature. We were able to identify distinct regions of the order map corresponding to LDA ($Q \geq 0.8, \tau > 0.46$), and HDA ($Q \leq 0.7, 0.43 < \tau < 0.5$), and to follow the evolution of structural order upon isobaric annealing. These results demonstrate the usefulness of an order metric approach in the quest for a more precise characterization of structural order in amorphous systems in general and water glasses in particular.

ACKNOWLEDGMENTS

We thank J.R. Errington for providing the numerical data shown in Fig. 5 of Ref. [8]. PGD and HES gratefully acknowledge the support of NSF through Collaborative Research in Chemistry Grant No. CHE 0404699. FS acknowledges the support of MIUR-Firb 2002.

APPENDIX

To test how sensitive the simulation results are to the method of preparation of LDA, we compare the compression of LDA prepared by *isochoric* cooling of the equilibrium liquid at $\rho = 0.9$ g/cm^3, with that of LDA prepared by *isobaric* cooling of equilibrium liquid at $P = 0.1$ GPa. In fact, this last procedure is the recipe followed in experiments to obtain hyperquenched-glassy water, HGW [51]. X-ray and neutron diffraction measurements suggest that LDA is structurally identical to HGW [52] and, although small differences have been found [53–55], the common view at present is that HGW and LDA are the same material [14,16,56].

Figure 9(a) shows the ρ-dependence of P when compressing both samples of LDA at $T = 77$ K. Both $P(\rho)$ curves behave in a qualitatively similar way. It can be seen that the two compression curves are similar, especially at high enough densities. Equation-of-state properties reveal some sensitivity to sample history at low densities.

Figure 9(b) shows the corresponding trace in the order map of the two compressions. We observe that both samples of LDA exhibit a very similar structural evolution. Therefore, Figure 9 suggests that our results do not depend strongly on the way in which LDA is prepared.

REFERENCES

[1] C. Kittel, *Introduction to Solid State Physics*, 7th ed. (Wiley, New York, 1996).

[2] R. Zallen, *The Physics of Amorphous Solids*, (Wiley, New York, 1983).

[3] S. Torquato, *Random Heterogeneous Materials: Microstructures and Macroscopic Properties* (Springer-Verlag, New York, 2002).

[4] S. Torquato, T.M. Truskett, and P.G. Debenedetti, Phys. Rev. Lett. **84**, 2064 (2000).

[5] T.M. Truskett, S. Torquato, and P.G. Debenedetti, Phys. Rev. E **62**, 993 (2000).

[6] J. R. Errington, P.G. Debenedetti, and S. Torquato, J. Chem. Phys. **118**, 2256 (2003).

[7] P.J. Steinhardt, D.R. Nelson, and M. Ronchetti, Phys. Rev. B **28**, 784 (1983).

[8] J.R. Errington and P.G. Debenedetti, Nature **409**, 318 (2001).

[9] G. Ruocco, M. Sampoli, A. Torcini, and R. Valluari, J. Chem. Phys. **99**, 8095 (1993); F.X. Prielmeier, E.W. Lang, R.J. Speedy, and H.-D. Lüdeman, Phys. Rev. Lett. **59**, 1128 (1987); C.A. Angell, E.D. Finch, L.A. Woolf, and P. Bach, J. Chem. Phys. **65**, 3063 (1976).

[10] F. W. Starr, F. Sciortino, and H.E. Stanley, Phys. Rev. E **60**, 6757 (1999).

[11] A. Scala, F.W. Starr, E. La Nave, F. Sciortino, and H.E. Stanley, Nature **406**, 166 (2000).

[12] P.G. Debenedetti, *Metastable Liquids, Concepts and Principles*, (Princeton University Press, Princeton, 1996).

[13] M.S. Shell, P.G. Debenedetti, and A.Z. Panagiotopoulos, Phys. Rev. E **66**, 011202 (2002).

[14] P.G. Debenedetti, J. Phys.: Condens. Matter **15**, R1669 (2003).

[15] C.A. Angell, Ann. Rev. Chem. **55**, 559 (2004).

[16] O. Mishima and H. E. Stanley, Nature **396**, 329 (1998).

[17] O. Mishima and L.D. Calvert, and E. Whalley, Nature **310**, 393 (1984).

[18] M. A. Floriano *et al.*, Y. P. Handa, D. D. Klug and E. Whalley, J. Chem. Phys. **91**, 7187 (1989).

[19] G.P. Johari, A. Hallbrucker, and Mayer, J. Phys. Chem. **94**, 1212 (1990).

[20] O. Mishima, L. D. Calvert and E. Whalley, Nature **314**, 76 (1985).

[21] O. Mishima, K. Takemura and K. Aoki, Science **254**, 406 (1991).

[22] O. Mishima, J. Chem. Phys. **100**, 5910 (1993).

[23] O. Mishima and H. E. Stanley, Nature **392**, 164 (1998).

[24] S. Klotz *et al.*, Phys. Rev. Lett. **94**, 025506 (2005).

[25] O. Mishima, Nature **384**, 546 (1996).

[26] N. Giovambattista, H.E. Stanley, and F. Sciortino, submitted; cond-mat/0502531.

[27] G. P. Johari and O. Andersson, J. Chem. Phys. **120**, 6207 (2004).

[28] C. A. Tulk, C. J. Benmore, J. Urquidi, D. D. Klug, J. Neuefeind, B. Tomberli and P. A. Egelstaff, Science **297**, 1320 (2002).

[29] R. Martoňák, D. Donadio, and M. Parrinello, Phys. Rev. Lett. **92**, 225702 (2004).

[30] N. Giovambattista, H.E. Stanley, and F. Sciortino, Phys. Rev. Lett. (to be published); cond-mat/0403365.

[31] B. Guillot and Y. Guissani, J. Chem. Phys. **119**, 11740 (2003).

[32] H.J.C. Berendsen, J.R. Grigera and T.P. Stroatsma, J. Phys. Chem. **91**, 6269 (1987).

[33] S. Harrington, P. H. Poole, F. Sciortino, and H. E. Stanley, J. Chem. Phys. **107**, 7443 (1997).

[34] F. Sciortino, L. Fabbian, S.-H. Chen, and P. Tartaglia, Phys. Rev. E **56**, 5397 (1997).

[35] N. Giovambattista, S.V. Buldyrev, F.W. Starr, and H.E. Stanley, Phys. Rev. Lett. **90**, 085506 (2003).

[36] F. Sciortino, P. Gallo, P. Tartaglia, and S.-H. Chen, Phys. Rev. E **54**, 6331 (1996).

[37] N. Giovambattista, H.E. Stanley, and F. Sciortino, Phys. Rev. Lett. **91**, 115504 (2003).

[38] H.J.C. Berendsen, J.P.M. Postma, W.F. van Gunsteren, A. DiNola, and J.R. Haak, J. Phys. Chem. **81**, 3684 (1984).

[39] N. Giovambattista, C.A. Angell, F. Sciortino, and H.E. Stanley, Phys. Rev. Lett **93**, 047801 (2004).

[40] N. Giovambattista, H.E. Stanley, and F. Sciortino, Phys. Rev. E **69**, 050201 (2004).

[41] P.L. Chau and A.J. Hardwick, Mol. Phys. **93**, 511 (1998).

[42] P. H. Poole, U. Essmann, F. Sciortino, and H. E. Stanley, Phys. Rev. E **48**, 4605 (1993).

[43] J.R. Errington, P.G. Debenedetti, and S. Torquato, J. Chem. Phys. **118**, 2256 (2003).

[44] S. Mossa and F. Sciortino, Phys. Rev. Lett. **92**, 045504 (2004).

[45] E. La Nave, S. Mossa, and F. Sciortino, Phys. Rev. Lett. **88**, 225701 (2002).

[46] W. Kob, F. Sciortino, and P. Tartaglia, Europhys. Lett. **49**, 590 (2000).

[47] S. Sastry, P.G. Debenedetti, and F.H. Stillinger, Nature **393**, 554 (1998).

[48] P. H. Poole, F. Sciortino, U. Essmann and H. E. Stanley, Nature **360**, 324 (1992).

[49] T. Loerting, C. Salzmann, I. Kohl, E. Mayer and A. Hallbrucker, Phys. Chem. Chem. Phys. **3**, 5355 (2001).

[50] J. L. Finney, D. T. Bowron, A.K. Soper, T. Loerting, E. Mayer and A. Hallbrucker, Phys. Rev. Lett. **89**, 205503 (2002).

[51] P. Brüggeller and E. Mayer, Nature **288**, 569 (1980).

[52] M.-C. Bellissent-Funel, L. Bosio, A. Hallbrucker, E. Mayer, and R. Sridi-Dorbez, J. Chem. Phys. **97**, 1282 (1992).

[53] G.P. Johari, A. Hallbrucker, and Mayer, Science **273**, 90 (1996).

[54] D.D. Klug, C.A. Tulk, E.C. Svensson, and C.-K. Loong, Phys. Rev. Lett. **83**, 2584 (1999).

[55] J.S. Tse, D.D. Klug, C.A. Tulk, I. Swainson, E.C. Svensson, C.-K. Loong, V. Shpakov, V.R. Belosludov, R.V. Belosludov, and Y. Kawazoe, Nature **400**, 647 (1999).

[56] P.G. Debenedetti and H.E. Stanley, Phys. Today **56**, 40 (2003).

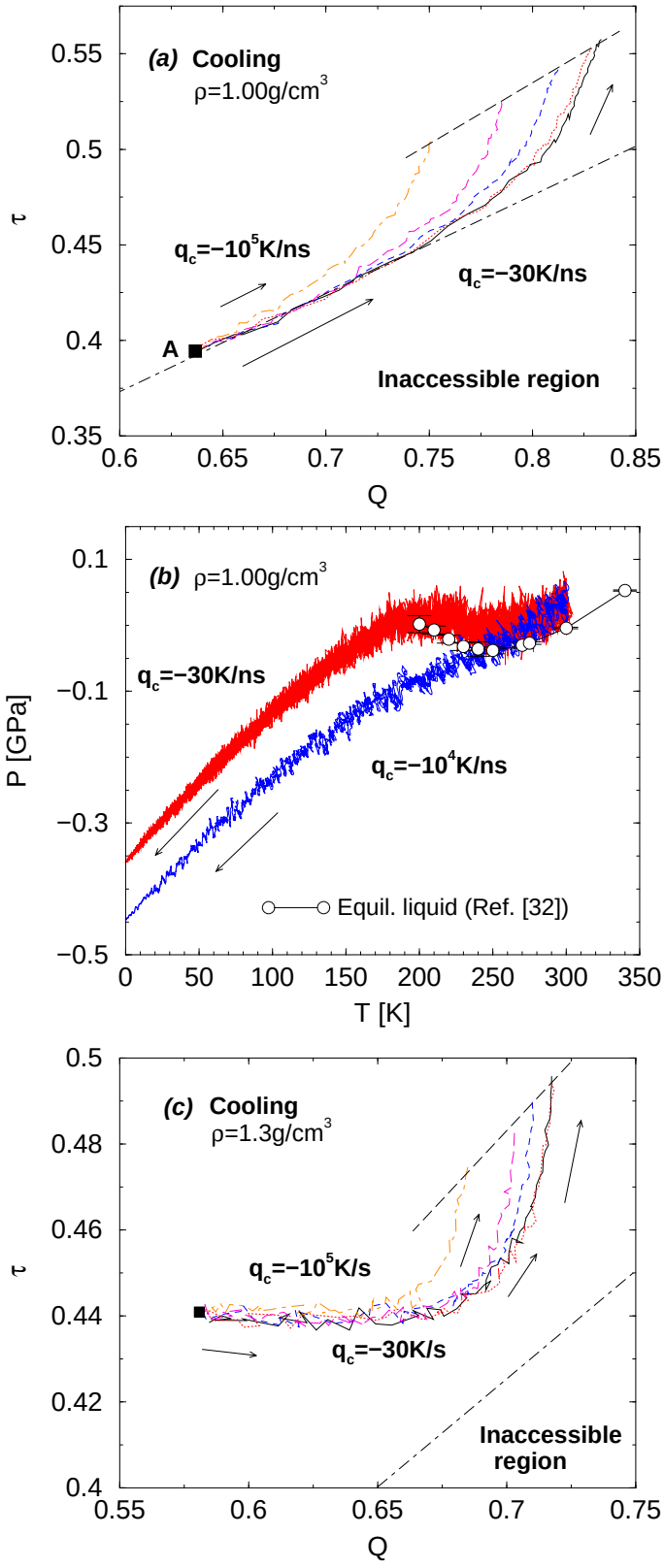

(a) Cooling
ρ=1.00g/cm3
qc=−10^5K/ns
qc=−30K/ns
A
Inaccessible region
τ
Q
(b) ρ=1.00g/cm3
qc=−30K/ns
qc=−10^4K/ns
Equil. liquid (Ref. [32])
P [GPa]
T [K]
(c) Cooling
ρ=1.3g/cm3
qc=−10^5K/s
qc=−30K/s
Inaccessible region
τ
Q

FIG. 1. (a) Behavior of the orientational and translational order parameters (Q and τ, respectively) when cooling an initially equilibrium liquid (point 'A': $T = 300$ K, $\rho = 1.0$ g/cm^3) at constant density $\rho = 1.00$ g/cm^3. Upon cooling at the slower rate, $q_c = -30$ K/ns, the system initially moves along the path corresponding to equilibrium $Q-\tau$ values (in (a), this path coincides with the dot-dashed line delimiting the inaccessible region for the liquid state). At lower T, the system deviates from the equilibrium path. The long-dashed line is the result of interpolating the Q-τ values of the glasses obtained at $T = 0$ K at different q_c. The various cooling rates correspond to q_c values of -10^5, -10^3, -10^3, -10^2 and -30 K/ns (left to right). (b) Pressure as a function of T upon cooling the liquid at $\rho = 1.00$ g/cm^3 for two different cooling rates. (c) Same as (a) for $\rho = 1.30$ g/cm^3.

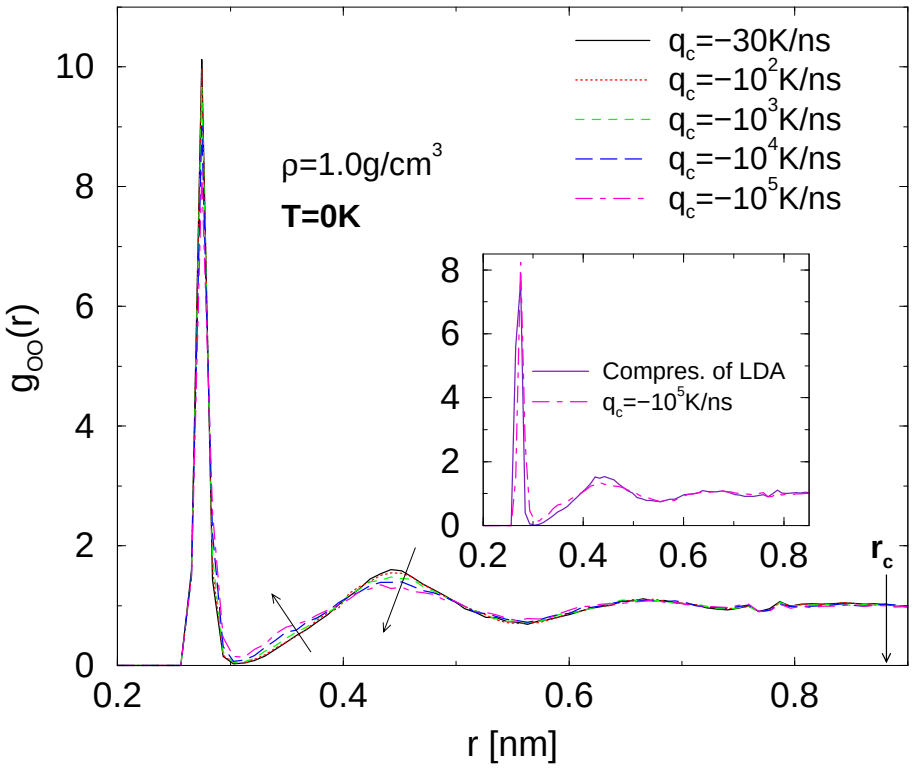
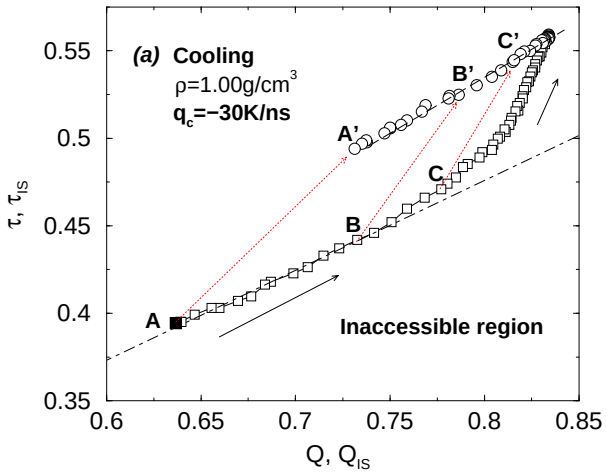
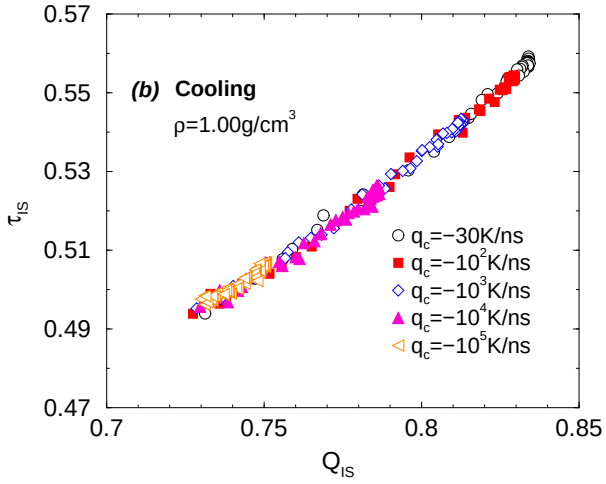
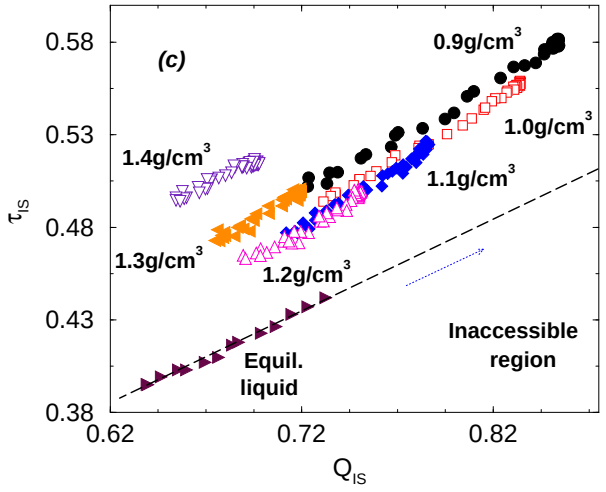


FIG. 2. Radial distribution function $g_{OO}(r)$ corresponding to the glasses at $T = 0$ K prepared by isochoric cooling at $\rho = 1.00$ g/cm^3 and different cooling rates. As the cooling rate increases (see arrows), mild changes in the first minimum and the second maximum of $g_{OO}(r)$ are observed indicating that molecules in the second shell move closer to the central molecule. These glasses show a very similar $g_{OO}(r)$ but have quite different order parameters [see Fig. 1(a)]. Same conclusion holds when comparing $g_{OO}(r)$ for the glass obtained upon $T = 0$ K-isothermal compression at $\rho = 1.0$ g/cm^3 and for the isochorically quenched glass at $q_c = -10^5$ K/ns at the same density and temperature (see inset). The cutoff value $\xi_c \equiv r_c \rho_n^{1/3}$ used in the definition of τ (see Eq. 1) corresponds to a cutoff distance $r_c = 0.883$ nm at $\rho = 1.0$ g/cm^3. The value of r_c is indicated by the arrow in the lower right corner.


(a) Cooling
ρ=1.00g/cm3
qc=−30K/ns
A
A'
B
B'
C
C'
Inaccessible region
τ, τIS
Q, QIS
0.55
0.5
0.45
0.4
0.35
0.6
0.65
0.7
0.75
0.8
0.85


(b) Cooling
ρ=1.00g/cm3
qc=−30K/ns
qc=−10^2K/ns
qc=−10^3K/ns
qc=−10^4K/ns
qc=−10^5K/ns
τIS
QIS
0.57
0.55
0.53
0.51
0.49
0.47
0.7
0.75
0.8
0.85


(c)
0.9g/cm3
1.0g/cm3
1.1g/cm3
1.2g/cm3
1.3g/cm3
1.4g/cm3
Equil. liquid
Inaccessible region
τIS
QIS
0.58
0.53
0.48
0.43
0.38
0.62
0.72
0.82

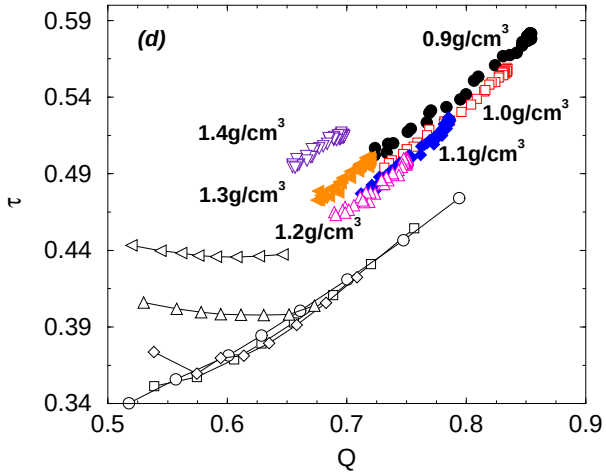


FIG. 3. (a) Order parameters Q and τ for the slowest cooling rate shown in Fig.1(a) (square symbols). For each configuration obtained upon cooling (e.g., points A, B, and C), we obtain the corresponding IS (points A', B', and C'). The order parameters in the IS (Q_{IS} and τ_{IS}), coincide with the long-dashed line obtained in Fig.1(a) for the glasses quenched at $T = 0$ K. (b) Location in the order map of the IS sampled upon cooling at different cooling rates. All IS fall on the same long-dashed line shown in (a). (c) Comparison of the location in the order map of the IS sampled at different densities at the slowest cooling rate studied, $q_c = -30$ K/ns. There is a line characterizing the location of the IS in the order map at each ρ. This line shifts in the order map non-monotonically with ρ. (d) Comparison between the IS lines shown in (c) and the lines obtained by the equilibrium liquid state points at different ρ [8] (shown at the lower left corner). At each density, the shape of the symbols (e.g., left-pointing triangles at $\rho = 1.3$ g/cm^3) is the same for the IS and the equilibrium liquid.

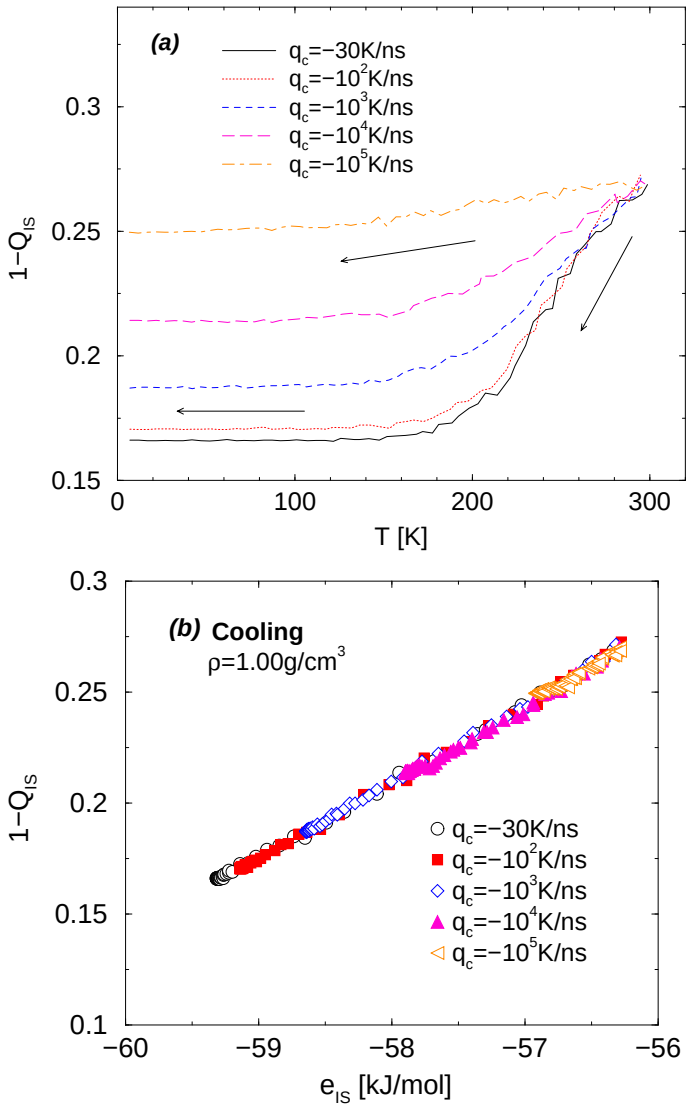


FIG. 4. (a) Orientational order parameter $1 - Q_{IS}$ in the IS as a function of temperature upon cooling at $\rho = 1.00$ g/cm^3 at different cooling rates. $1 - Q_{IS}(T)$ behaves similarly to the energy of the IS observed in [40] under same conditions. (b) Q_{IS} as a function of the energy of the IS, e_{IS}, suggesting that $1 - Q_{IS} \approx e_{IS}$, independently of the cooling rate. Similar results are found at all densities studied.

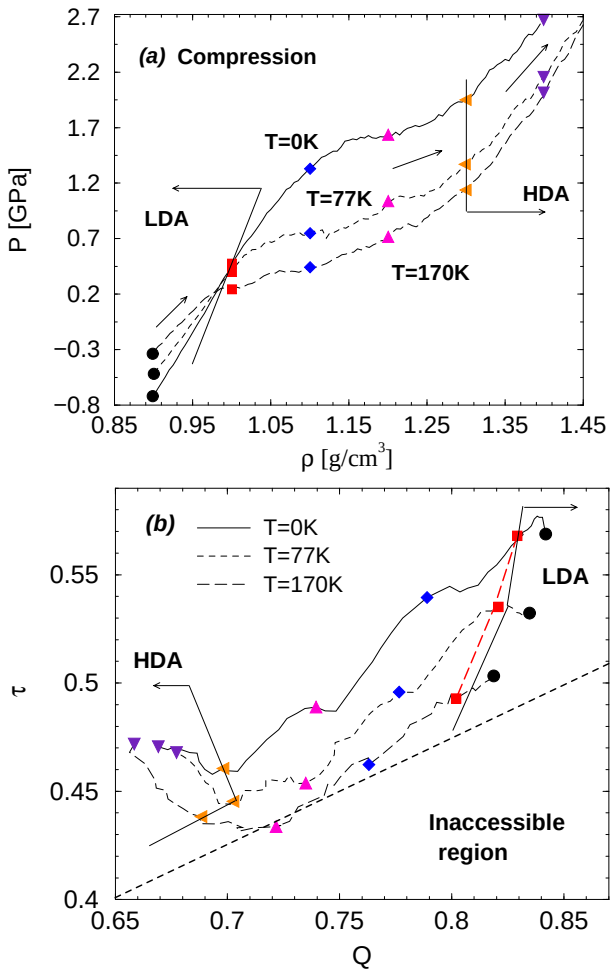


FIG. 5. (a) Evolution of pressure with density upon compression of low-density amorphous ice (LDA) to produce high-density amorphous ice (HDA). Compression is performed at $T = 0$, 77, and 170 K, below the glass transition temperature. We indicate approximately the location corresponding to LDA and HDA. (b) Order parameters of the glasses sampled along the isotherms shown in (a). The location in the order map corresponding to LDA and HDA is also indicated. Filled symbols correspond to the glasses obtained at $\rho = 0.9$ up to 1.4 g/cm^3 in steps of 0.1 g/cm^3.

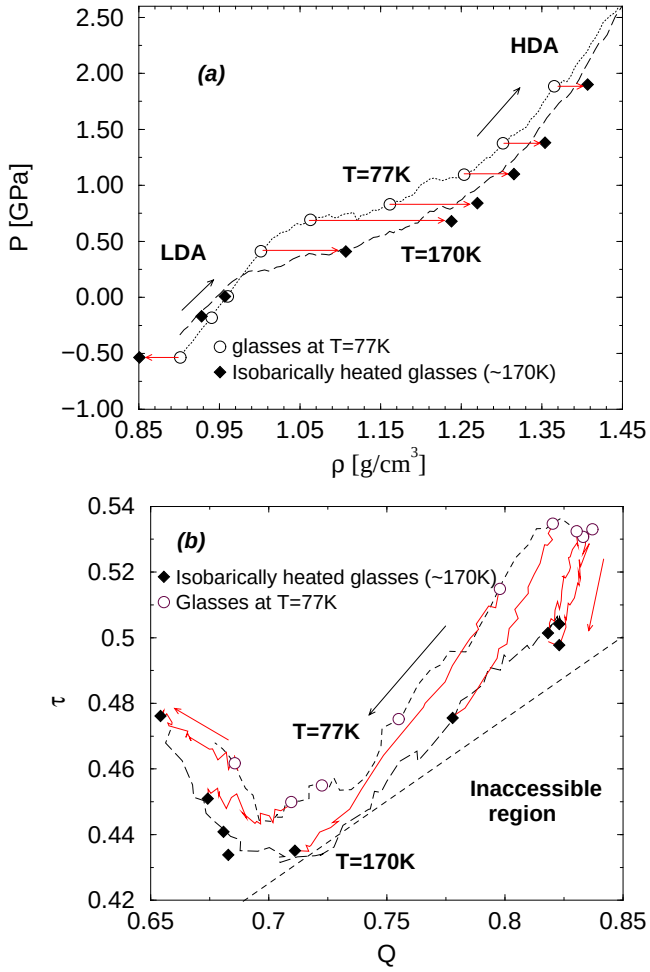


FIG. 6. (a) Evolution of pressure with density upon compression of low-density amorphous ice (LDA) to produce high-density amorphous ice (HDA). Compression is performed at $T = 77$, and 170 K. Selected glasses at $T = 77$ K (open circles) are annealed/isobarically heated up to $T \approx 170$ K (filled diamonds); see horizontal arrows. The annealed glasses in the $P - \rho$ plane approach or cross the $T \approx 170$ K-isotherm. (b) Location in the order map of the glasses indicated in (a). Density increases from right to left along both isotherms.

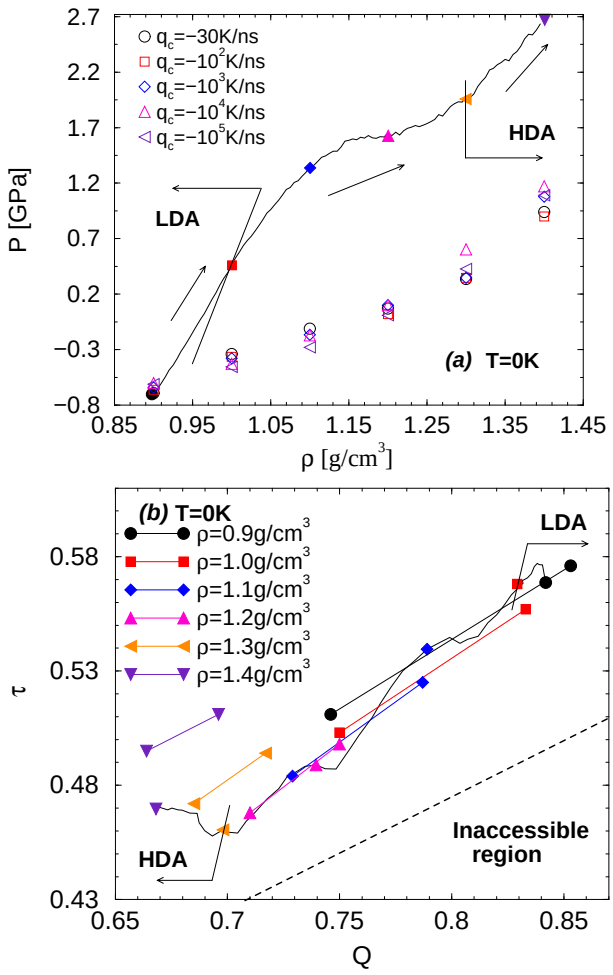


FIG. 7. (a) Comparison of the location in the $P-\rho$ plane of the glasses at $T=0$ K obtained by isothermal compression of LDA and by isochorically cooling at different densities and cooling rates. At $T=0$ K no annealing is possible. Open symbols represent different cooling rates while solid symbols on the $T=0$ K-isotherm correspond to glasses from $\rho=0.9$ g/cm^3 to $\rho=1.4$ g/cm^3 in steps of 0.1 g/cm^3. (b) Location in the order map of the glasses indicated in (a). Glasses formed by isochoric cooling lie on the straight lines connecting fast- (low-Q end) and slow-cooled (high-Q end) extremes at each density. We also show the location of the glasses along the $T=0$ K-isotherm indicated in (a).

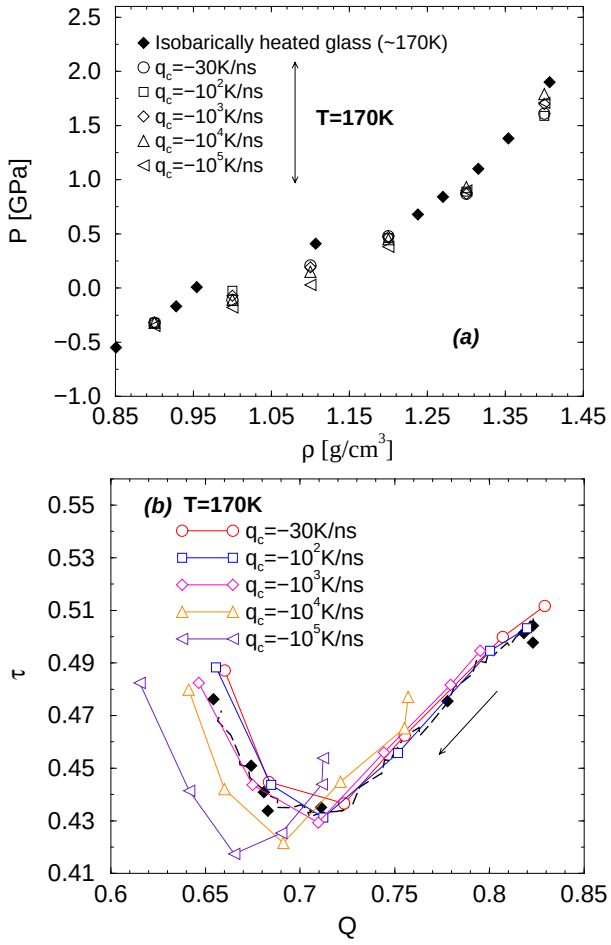


FIG. 8. (a) Comparison of the location in the $P-\rho$ plane of the glasses at $T = 170$ K obtained by isochoric cooling at different densities and cooling rates (open circles), and by annealing/isobarically heating of glasses obtained by compression of LDA at $T = 77$ K (solid diamonds) [see Fig. 6(a)]. (b) Location in the order map of the glasses indicated in (a). Lines connecting open symbols correspond to glasses obtained at a given cooling rate for different densities [density increases from 0.9 g/cm^3 (high-Q values) to 1.4 g/cm^3 (low-Q values), in steps of 0.1 g/cm^3]. For comparison, we also show the location of the glasses obtained by isothermal compression ($T = 170$ K) of LDA (long-dashed line). We note that all glasses in (b) are at $T = 170$ K and, therefore, they have the same vibrational contributions.

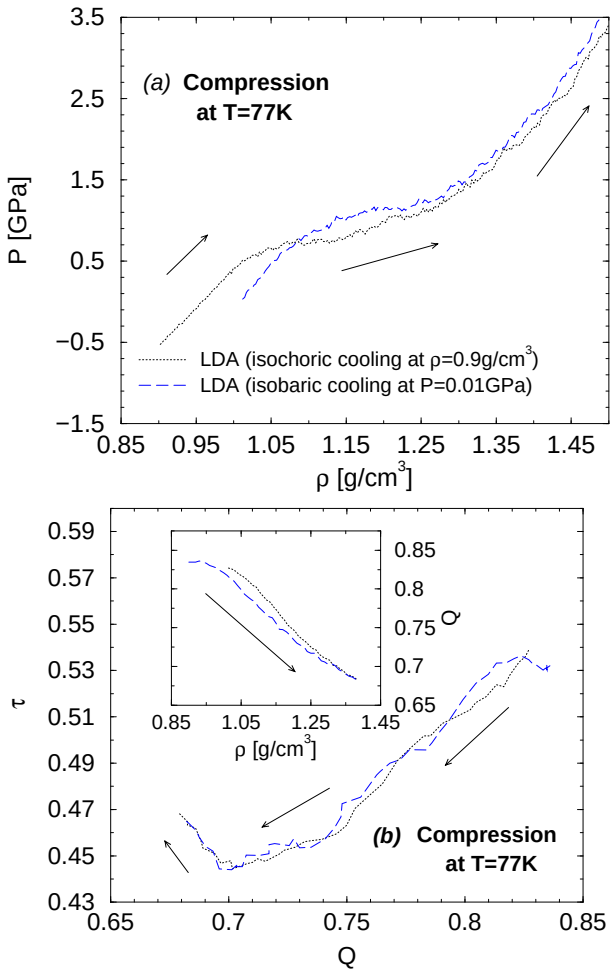


FIG. 9. Comparison of the ρ-dependence upon compression for two samples of LDA prepared in a different way: LDA obtained by isochoric fast-cooling of equilibrium liquid at $T = 220$ K and $\rho = 0.9$ g/cm^3, and LDA obtained by isobaric slow-cooling at $P = 0.01$ GPa. (b) Comparison of the order parameters in the glasses sampled upon compression both samples of LDA shown in (a). Results are qualitatively similar in both cases suggesting that the preparation of LDA does not alter our conclusions.